Journal of Power Sources 182 (2008) 145–152

Contents lists available at ScienceDirect

Journal of Power Sources

journal homepage: www.elsevier.com/locate/jpowsour

An investigation into nickel implanted 316L stainless steel as a bipolar plate for PEM fuel cell

Kai Feng[a], Yao Shen[a,*], Jianming Mai[b], Dongan Liu[b], Xun Cai[a]

[a] Shanghai Key Laboratory of Materials Laser Processing and Modification, School of Materials Science and Engineering, Shanghai Jiao Tong University, Shanghai 200240, PR China
[b] School of Mechanics and Engineering, Shanghai Jiao Tong University, Shanghai 200240, PR China

ARTICLE INFO

Article history:
Received 9 February 2008
Received in revised form 28 March 2008
Accepted 31 March 2008
Available online 18 April 2008

Keywords:
Bipolar plate
Polymer electrolyte membrane fuel cell
Ion implantation
Corrosion
316L stainless steel

ABSTRACT

A nickel-rich layer about 100 μm in thickness with improved conductivity was formed on the surface of austenitic stainless steel 316L (SS316L) by ion implantation. The effect of ion implantation on the corrosion behavior of SS316L was investigated in 0.5 M H_2SO_4 with 2 ppm HF solution at 80 °C by potentiodynamic test. In order to investigate the chemical stability of the ion implanted SS316L, the potentiostatic test was conducted in an accelerated cathode environment and the solutions after the potentiostatic test were analyzed by inductively coupled plasma atomic emission spectrometer (ICP-AES). The results of potentiodynamic test show that the corrosion potential of SS316L is shifted toward the positive direction from −0.3 V versus SCE to −0.05 V versus SCE in anode environment and the passivation current density at 0.6 V is reduced from 11.26 to 7.00 μA cm^{-2} in the cathode environment with an ion implantation dose of 3×10^{17} ions cm^{-2}. The potentiostatic test results indicate that the nickel implanted SS316L has higher chemical stability in the accelerated cathode environment than the bare SS316L, due to the increased amount of metallic Ni in the passive layer. The ICP results are in agreement with the electrochemical test results that the bare SS316L has the highest dissolution rate in both cathode and anode environments and the Ni implantation markedly reduces the dissolution rate. A significant improvement of interfacial contact resistance (ICR) is achieved for the SS316L implanted with nickel as compared to the bare SS316L, which is attributed to the reduction in passive layer thickness caused by the nickel implantation. The ICR values for implanted specimens increase with increasing dose.

© 2008 Elsevier B.V. All rights reserved.

1. Introduction

The polymer electrolyte membrane fuel cell (PEMFC) is one of the most promising power sources for transportation and distributed power generation. As an electrochemical device that converts the chemical energy stored in fuels into electrical energy directly [1], it offers many advantages such as high efficiency and zero-emission as compared to traditional power sources [2]. Since every single cell can only create a potential of about 0.6 V, it is necessary to assemble many fuel cells into a stack with bipolar plates to increase the power output.

The main function of bipolar plate is to connect the cathode side of one cell with the anode side of the other and to separate the reactive gases between the anode side (hydrogen gas) and cathode side (oxygen gas). Good corrosion resistance, high electrical conductivity, good mechanical performance, high gas impermeability and low cost are required for practical applications of the bipolar plate materials. Graphite has been used as the bipolar plate material due to its good corrosion resistance and high electrical conductivity. However, graphite is neither suitable for transportation applications that demand good structural durability against shock and vibration nor suitable for large-scale manufacturing because of its poor mechanical strength [3].

In contrast to graphite, metallic materials can be used as bipolar plates because of their good mechanical strength, high gas impermeability, low cost and ease of manufacturing [4–13]. Stainless steel is considered as one of the promising candidates. However, surface modification is necessary for stainless steel to be used for the bipolar plate in PEMFC because of two major challenges. One is to further improve its corrosion resistance especially in cathode environment in PEMFC, although stainless steel is famous for its high corrosion resistance in common applications. This is because metallic ions produced by corrosion of metal can permeate to the membrane and degrade its performance [14–16]. The other challenge is the passive layer formed in PEMFC environment which can lower the electrical conductivity of the bipolar plate [17,18].

* Corresponding author. Tel.: +86 21 3420 3763; fax: +86 21 3420 3763.
E-mail address: yaoshen2001@yahoo.com (Y. Shen).

0378-7753/$ – see front matter © 2008 Elsevier B.V. All rights reserved.
doi:10.1016/j.jpowsour.2008.03.088

Ion implantation is widely used to modify surface properties such as the mechanical and tribological properties. Unlike in other thermodynamics limited processes such as diffusion and phase transformation, the quantity of the elements that can be ion implanted is not restricted by solubility and phase diagrams [19]. The elements beneficial to corrosion resistance, such as Ni, Mo and Cr, can be greatly enriched in the surface layer by ion implantation to improve the corrosion resistance [20,21]. In the present work, SS316L was implanted with nickel and the corresponding effects on its corrosion resistance in PEMFC environment and its interfacial contact resistance (ICR) were investigated.

2. Experimental

2.1. Materials and ion implantation

Stainless steel 316L of 6 mm in thickness were used as the substrate. The steel plates were cut into 15 mm × 15 mm specimens for ion implantation and subsequent tests. Before ion implantation, the specimens were polished with Al_2O_3 waterproof abrasive paper and were degreased with acetone in an ultrasonic cleaner and dried afterwards.

The ion implantation was carried out in a home-designed multifunctional ion implantation apparatus. The vacuum level of the MEVVA (metal vapor vacuum arc) implantation target chamber was 3.0×10^{-3} Pa. The extraction voltage was 20 kV. The specimens were implanted for 1×10^{17}, 2×10^{17}, 3×10^{17}, 4×10^{17} and 5×10^{17} ions cm^{-2}, respectively.

2.2. XPS analysis and surface topography

Kratos AXIS Ultra X-ray photoelectron spectroscopy (XPS) was employed to analyze the composition profiles of the elements Fe, Ni, Cr and O in the implanted layer, with the accuracy in the concentration measurement being 1%. The specimens were sputtered at 4.5 nm min^{-1} with Al Kα source. The chemical species of Ni and Cr in the bare and nickel implanted SS316L were analyzed, with the binding energy of the elements normalized by that of carbon, 284.8 eV. The surface topography of nickel implanted samples was measured with an atomic force microscope (AFM).

2.3. Electrochemical measurements

The potentiodynamic and potentiostatic test were conducted to evaluate the electrochemical behavior of the bare and the nickel implanted specimens with doses ranging from 1×10^{17} to 5×10^{17} ions cm^{-2}. All specimens were embedded in epoxy resin with an exposed surface of 1 cm^2. A three-electrode system was used for the electrochemical measurements, in which a platinum sheet worked as the counter electrode, a saturated calomel electrode (SCE) as the reference electrode and the specimen as the working electrode. All electrochemical measurements were conducted in 0.5 M H_2SO_4 with 2 ppm HF solution at 80 °C with CHI 606C Electrochemical Analyzer. The potentiodynamic polarization was measured in the range from −0.6 V versus SCE to 1.0 V versus SCE with a potential scanning rate of 1 mv s^{-1} after 30 min immersion in the solution. The potentiostatic test was carried out to investigate the performance and stability of the bare and the nickel implanted specimens in the accelerated cathode environment. The potentiostatic test was conducted at the potential of 0.6 V versus SCE for 10000 s with air bubbling to simulate the cathode environment in PEMFC.

After potentiostatic test, the solutions (10–15 ml) were collected and analyzed by inductively coupled plasma atomic emission spectrometer (ICP-AES) to quantify the metallic Fe, Cr, Ni and Mo ions dissolved into the solutions. A solution containing 1 ppm of each of the metal ions in 0.5 M H_2SO_4 was purchased from SPEX CertiPrep Inc. as a standard solution. Due to the variability in the plasma, pump rate and nebulizer efficiency, ICP has a error bar of 5%.

2.4. Interfacial contact resistance

The interfacial contact resistance of the bare and the nickel implanted specimens were evaluated by the method described in ref. [14]. Briefly, it was a sandwiched structure using two pieces of conductive carbon paper that were sandwiched between the sample and two copper plates. A constant current (0.1 A) was applied via the two copper plates, and the variation in the total voltage was recorded with respect to the compaction force that was steadily increased. The measured resistance for the system was expressed as follows:

$$R_{\text{Total}} = 2R_{\text{copper-wire}} + 2r_{\text{copper-CP}} + 2R_{\text{CP}} + 2r_{\text{SS-CP}} + R_{\text{sample}} \quad (1)$$

where R represent the respective bulk resistance and r is the interfacial contact resistance between the respective contact pair. In particular, $R_{\text{copper-wire}}$, R_{CP} and R_{sample} are, respectively, the sum of the bulk resistances of the copper plate and the wire, the bulk resistance of the carbon paper and the bulk resistance of the SS316L, and $r_{\text{copper-CP}}$ and $r_{\text{SS-CP}}$ are, respectively, the interfacial contact resistance between the copper plate and the carbon paper and the interfacial contact resistance between the SS316L sample and the carbon paper. When one piece of the carbon paper is sandwiched with two copper plates, the resistance of this new system is measured by

$$R_{\text{base}} = 2R_{\text{copper-wire}} + 2r_{\text{copper-CP}} + R_{\text{CP}} \quad (2)$$

Since R_{sample} was much smaller than other resistances, we assume that it was negligible. And R_{CP} was obtained from the supplier. Thus, ICR between the SS316L and the carbon paper ($r_{\text{SS-CP}}$) can be calculated from Eqs. (1) and (2). For the nickel implanted SS316L samples, the ICR between the Ni-implanted surface and the carbon paper was measured by the same procedure with the ICR between the bare backside and the carbon paper ($r_{\text{SS-CP}}$) being the same as that for the bare SS316L sample.

3. Results and discussion

3.1. XPS and surface topography analysis

Fig. 1 shows the XPS depth profiles of the bare SS316L and the nickel implanted with doses of 1×10^{17}, 3×10^{17} and 5×10^{17} ions cm^{-2}, respectively. It can be seen that a nickel-rich layer about 100 nm in thickness was formed in the near-surface region as shown in Fig. 1b–d, with the peak atomic fraction of nickel being 24.2, 29.1 and 34.7%, respectively, all at a depth of approximately 18 nm. It is noted that the thickness of the oxide layer in the nickel implanted SS316L sample (about 18 nm) is significantly smaller than that in the bare sample (about 50 nm).

The species of Ni and Cr in the nickel-rich layer before and after ion implantation with a dose of 3×10^{17} ions cm^{-2} were analyzed by XPS. The results are shown in Figs. 2 and 3. The evolution of Ni and Cr before and after sputtering for 120 s are summarized in Tables 1 and 2, respectively. It can be seen from Fig. 2a that NO and $Ni(OH)_2$ are dominant species, but little amount of metallic Ni is present in the outer layer. After Ar^+-sputtering for 120 s the Ni_{met} and NiO are dominant and no $Ni(OH)_2$ is present (Fig. 2b). These results are similar to those reported in an investigation of passive films formed on Ni in a H_2SO_4 solution [22], which indicates an outer layer consisting of a nickel hydroxide and an inner layer of

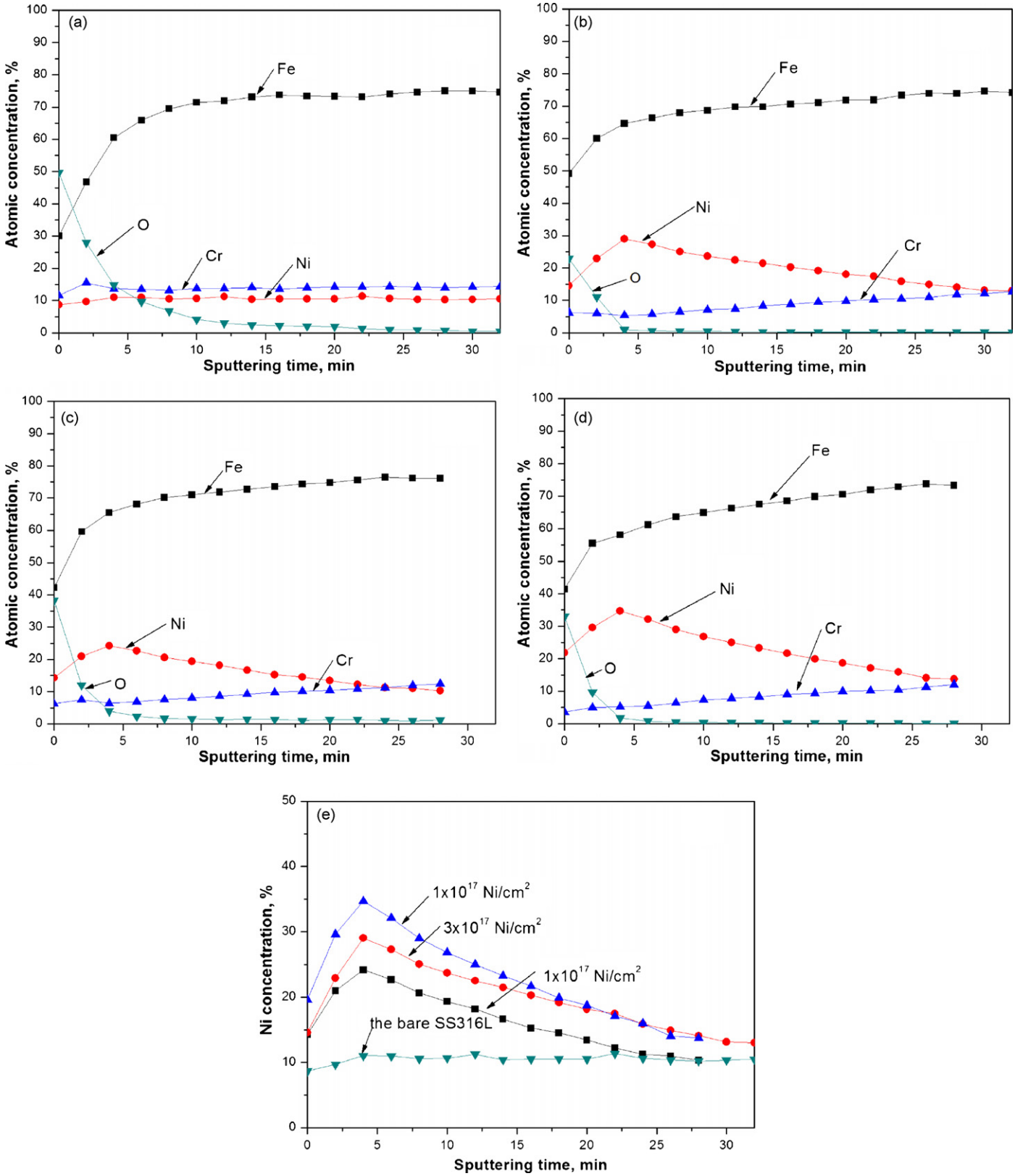

Fig. 1. XPS depth profiles for the bare and nickel implanted SS316L. (a) Fe, Ni, Cr and O concentrations for the bare SS316L (b) for 1×10^{17} ions cm^{-2}, (c) for 3×10^{17} ions cm^{-2}, (d) for 5×10^{17} ions cm^{-2} and (e) Ni concentration for the bare and three doses of SS316L. The sputtering rate is 4.5 nm min^{-1}.

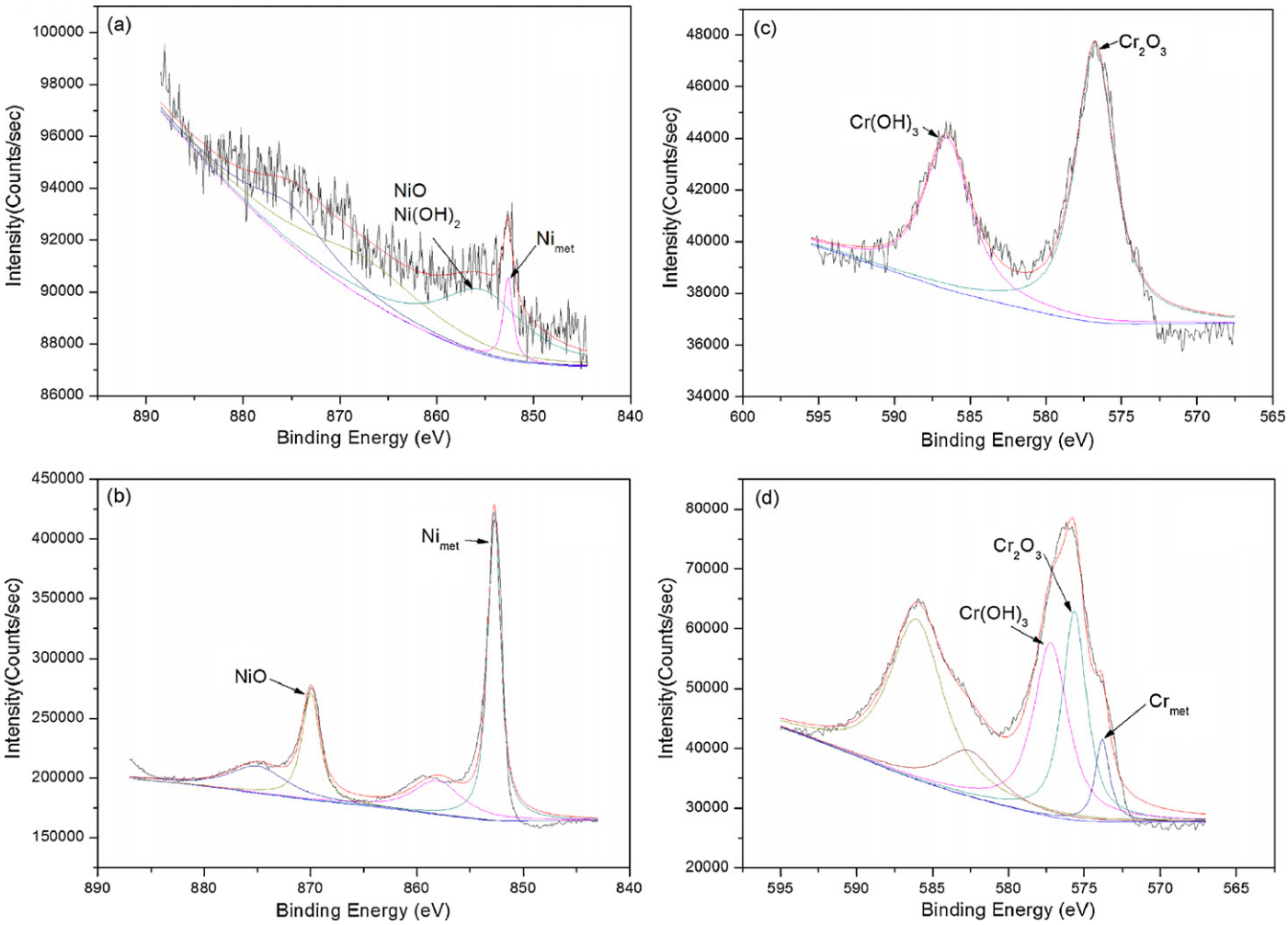

Fig. 2. Ni and Cr XPS spectra for the bare SS316L (a) Ni before sputtering, (b) Ni sputtering for 120 s, (c) Cr before sputtering and (d) Cr sputtering for 120 s.

nickel oxide. The Cr species before sputtering consist of 60% Cr_2O_3 and 40% $Cr(OH)_3$ (Fig. 2c). After sputtering for 120 s, the contribution of Cr_2O_3 decreases to 42%, while that of $Cr(OH)_3$ increases to 48%, with the appearance of metallic Cr (Fig. 2d).

After the nickel implantation, the Ni species and their concentrations are identified as metallic nickel (Ni, 23%), divalent nickel oxide (NiO, 41%) and divalent nickel hydroxide ($Ni(OH)_2$, 36%) by the respective binding energies of approximately 853, 855 and 856.3 eV corresponding to the three main peaks in the curve fitting to the Ni spectrum. It is noted that the contribution of Ni_{met} increases to 23% in the outer layer over that of the bare SS316L. After sputtering for 120 s, the Ni spectrum (Fig. 3b) is fitted with two main peaks with no obvious difference in the details of the curve fitting comparing to those for the un-implanted specimens (Fig. 2b). For Cr in the nickel implanted SS316L, as compared to that of the bare specimen, the contribution of Cr_2O_3 in the outer layer increases from

Table 1
Evolution of Ni contributions for the bare and nickel implanted with dose of 3×10^{17} ions cm^{-2} SS316L in function of erosion times

	The bare SS316L		Nickel implanted SS316L	
	Ni	Ni species	Ni	Ni species
Before sputtering				
Energy (eV)	852.5	Ni_{met}	853	Ni_{met}
Contribution (%)	13		23	
Energy (eV)	855.6	NiO	855	NiO
Contribution (%)	87	$Ni(OH)_2$	41	
Energy (eV)			856.3	$Ni(OH)_2$
Contribution (%)			36	
Sputtering for 120 s				
Energy (eV)	852.5	Ni_{met}	852.5	Ni_{met}
Contribution (%)	67		68	
Energy (eV)	871.8	NiO	871.8	NiO
Contribution (%)	33		32	

Table 2
Evolution of Cr contributions for the bare and nickel implanted with dose of 3×10^{17} ions cm^{-2} SS316L in function of erosion times

	The bare SS316L		Nickel implanted SS316L	
	Cr	Cr species	Cr	Cr species
Before sputtering				
Energy (eV)	576.8	Cr_2O_3	576.8	Cr_2O_3
Contribution (%)	60		67	
Energy (eV)	586.8	$Cr(OH)_3$	586.8	$Cr(OH)_3$
Contribution (%)	40		33	
Sputtering for 120 s				
Energy (eV)	573.8	Cr_{met}	574.2	Cr_{met}
Contribution (%)	10		25	
Energy (eV)	575.9	Cr_2O_3	575.9	Cr_2O_3
Contribution (%)	42		27	
Energy (eV)	577.3	$Cr(OH)_3$	577.3	$Cr(OH)_3$
Contribution (%)	48		48	

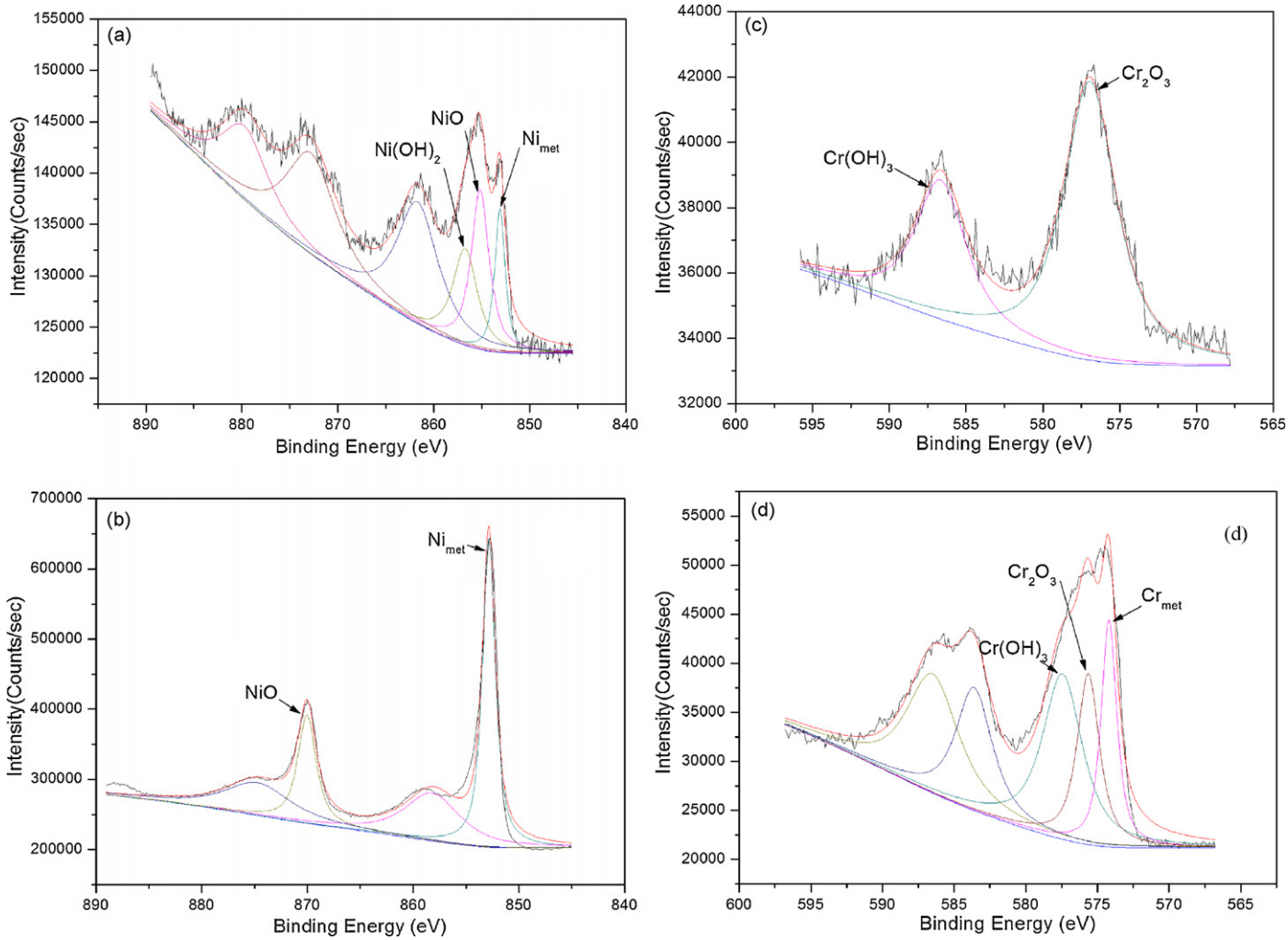

Fig. 3. Ni and Cr XPS spectra for the nickel implanted (3×10^{17} ions cm^{-2}) SS316L (a) Ni before sputtering, (b) Ni sputtering for 120 s, (c) Cr before sputtering and (d) Cr sputtering for 120 s.

60 to 67%, while in the inner layer (after sputtering for 120 s) the contributions of chromium oxide and hydroxide decrease from 90 to 75%.

The surface roughness increases with increasing dose as shown by the AFM images of the nickel implanted SS316L (Fig. 2). The surface roughness (R_a) is 0.12, 0.35 and 1.22 nm, respectively, for the specimens implanted with doses of 1×10^{17}, 3×10^{17} and 5×10^{17} ions cm^{-2}.

3.2. Potentiodynamic test

The potentiodynamic polarization behavior of the bare and the nickel implanted SS316L in 0.5 M H_2SO_4 with 2 ppm HF solution at 80 °C are presented in Fig. 5. Fig. 5a and b shows the potentiodynamic polarization results in the accelerated anode (H_2 bubbled) and cathode (air bubbled) environment, respectively. In general, all the SS316L in the PEMFC environment, bare or nickel implanted, exhibit a typical polarization curve that consists of three regions, i.e., active region, passivation region and transpassive region. In the PEMFC anode environment, it can be seen that the corrosion potential (E_{corr}) of SS316L is close to −0.3 V versus SCE. After nickel implantation, the passivation region narrowed by about 20% and E_{corr} in the anode environment was shifted toward the positive direction and reached about −0.05 V versus SCE (Fig. 3a), more positive than the PEMFC anode operation potential of about −0.1 V versus SCE, implying that the anode operation potential is cathodic to nickel implanted SS316L. For SS316L, the nickel implantation has a significant influence on the peak passivating current, reducing it by two orders of magnitude, while shifting the passivating potential 0.25 anodic (from −0.20 V versus SCE to 0.05 V versus SCE). Note that the nickel implantation with a dose of 3×10^{17} ions cm^{-2} decreases the passivation current density from 11.73 to about 5 μA cm^{-2}. When the potential is higher than 0.9 V versus SCE, the current density increase rapidly for all the specimens due to the dissolution of the passive film.

The corrosion potential (E_{corr}) in the cathode environment (Fig. 5b) also shifted toward the positive direction after nickel implantation. The same as the SS316L, the current density increased dramatically when the potential reached about 0.9 V versus SCE. Fortunately, the PEMFC cathode operation potential (0.6 V versus SCE) is in the passivation region, in which a stable passive film is formed on the surface. The passivation current density for the bare and the nickel implanted SS316L at 0.6 V versus SCE is listed in Table 3. The passivation current density of SS316L in the cathode operation potential (0.6 V versus SCE) is 11.26 μA cm^{-2}. For low ion implantation doses, the current density at 0.6 V versus SCE decrease with increasing nickel implantation dose. When the dose is 1×10^{17}, 2×10^{17} and 3×10^{17} ions cm^{-2}, the current density at the

Table 3
The passivation current density ($\mu A\,cm^{-2}$) for the bare and nickel implanted SS316L at 0.6 V vs. SCE (PEMFC cathode environment)

Bare SS316L	1×10^{17} Ni cm^{-2}	2×10^{17} Ni cm^{-2}	3×10^{17} Ni cm^{-2}	4×10^{17} Ni cm^{-2}	5×10^{17} Ni cm^{-2}
11.26	7.91	7.28	7.00	7.02	7.89

cathode operation potential is 7.91, 7.28 and 7.00 $\mu A\,cm^{-2}$, respectively. The current density for the SS316L nickel implanted with a dose of 3×10^{17} ions cm^{-2} is reduced by more than one third as compared to that for the bare specimen, which implies that the ion implantation of Ni could effectively decrease the corrosion rate of the passive film. This could be attributed to the increase of metallic Ni in the passive layer. As the exchange current of hydrogen is relatively small with nickel, the nickel implanted SS316L, which contain more metallic Ni than the bare SS316L, can maintain the passivation current density at a lower level when the polarization potential is increased. However, when the dose is 4×10^{17} or 5×10^{17} ions cm^{-2}, the current density increased to 7.02 and 7.89 $\mu A\,cm^{-2}$, respectively. It is easy to understand the slight increase of the current density from the AFM images (Fig. 4c). The ion implantation deteriorated the surface integrity and created flaws and defects which would accelerate the corrosion rate.

3.3. Potentiostatic test and ICP measurements

As can be seen from the potentiodynamic test results (Fig. 5a), the anode environment is protective for the nickel implanted SS316L, so the potentiostatic test was conducted to examine the current density for a long-term operation only in the cathode environment. The current density as a function of time is recorded and plotted in Fig. 6. The current density of all specimens decreased rapidly in the beginning and then was gradually stabilized. This reduction in the current density reflects the formation of the passive film on the surface. For the bare

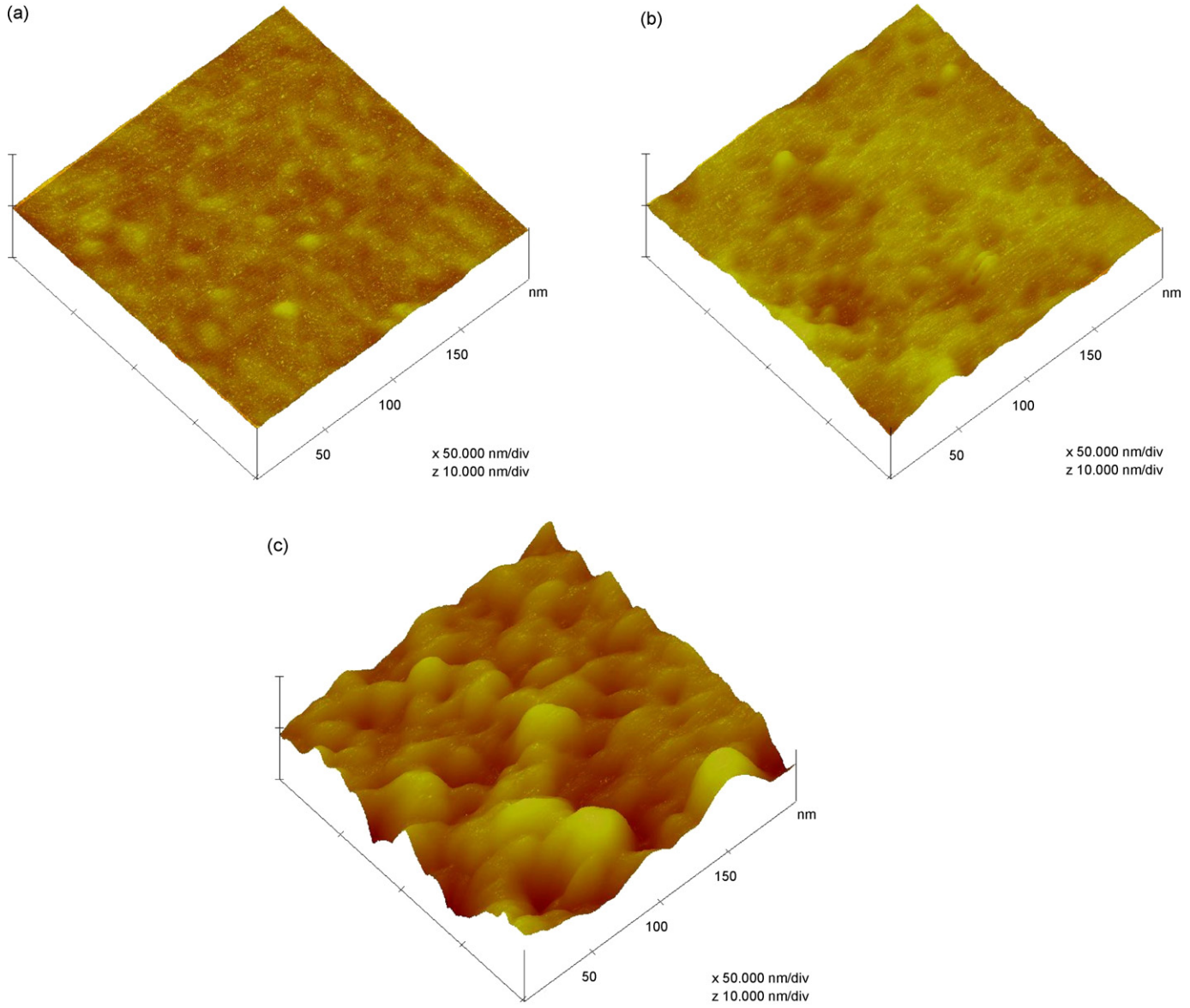

Fig. 4. AFM images (tapping mode) of the nickel implanted SS316L. (a) 1×10^{17} ions cm^{-2}, (b) 3×10^{17} ions cm^{-2} and (c) 5×10^{17} ions cm^{-2}.

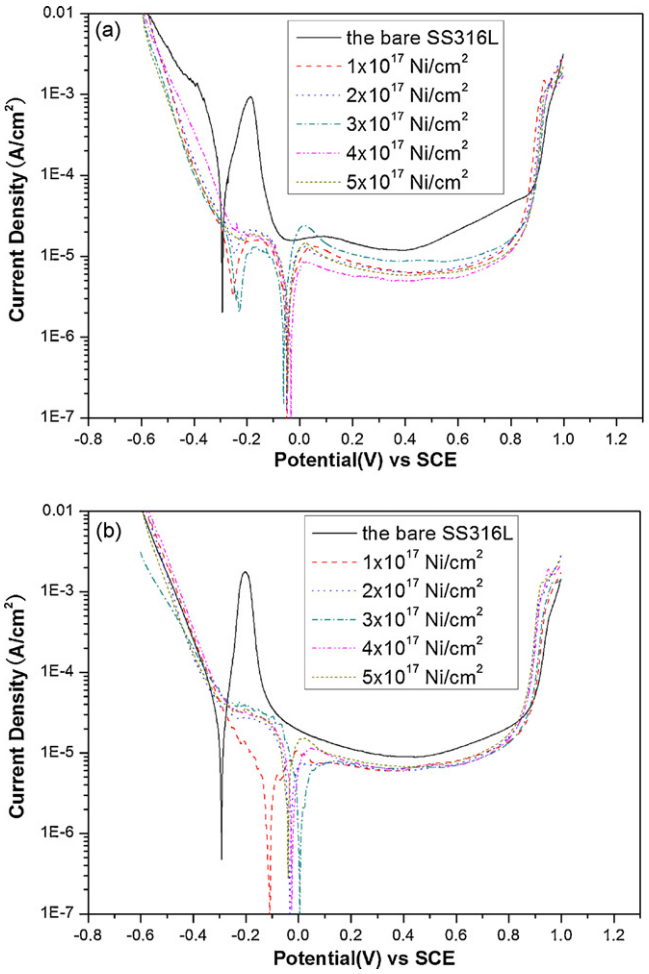

Fig. 5. Polarization curves for the bare and the nickel implanted SS316L in 0.5 M H_2SO_4 with 2 ppm HF at 80 °C: (a) bubbled with H_2 and (b) bubbled with air.

SS316L, the stabilized current density is relatively high as of 10 μA cm^{-2}. But for the nickel implanted specimens, they are quite low, being 1.3, 1.0, 0.8, 1.4 and 2.1 μA cm^{-2} at the end of the experiment, for the respective dose in increasing order. These are in agreement with the polarization curves (Fig. 5b) in which the current density decrease as the ion implantation

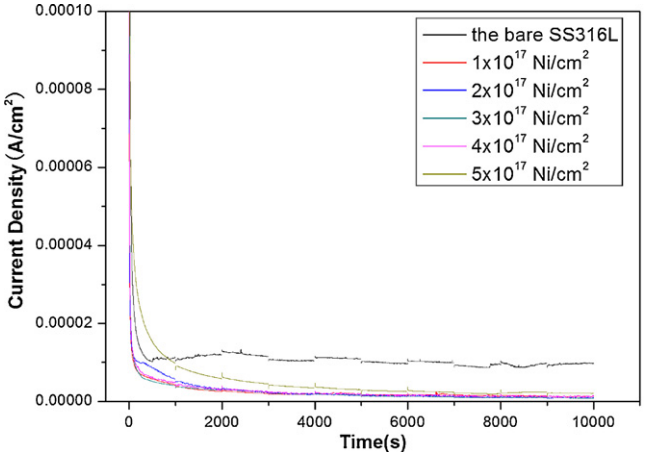

Fig. 6. Transient currents of the bare and the nickel implanted SS316L at 0.6 V vs. SCE in 0.5 M H_2SO_4 with 2 ppm HF at 80 °C bubbled with air (cathode environment).

Table 4
Fe, Ni, Cr, Mo ion concentrations for the bare and nickel implanted SS316L after potentiostatic test in PEMFC cathode environment (averaged for three samples)

	Ion concentration in PEMFC cathode environment after 10,000 s (ppm)			
	Fe	Ni	Cr	Mo
Bare SS316L	2.94	1.53	0.37	0.06
1×10^{17} Ni cm^{-2}	1.28	0.29	0.04	0.02
2×10^{17} Ni cm^{-2}	0.91	0.18	0.03	0.02
3×10^{17} Ni cm^{-2}	0.34	0.04	<0.01	–
4×10^{17} Ni cm^{-2}	0.61	0.09	<0.01	–
5×10^{17} Ni cm^{-2}	1.16	0.14	0.05	0.02

dose increase and reach its minimum when the dose became 3×10^{17} ions cm^{-2}.

The solutions after potentiostatic test for 10,000 s were collected and the metal ions dissolved were analyzed by ICP and the results are summarized in Table 4. Fe is found in the highest concentration in all cases, due to its high concentration in the SS316L and its selective dissolution [23]. The bare SS316L yield the highest concentrations of Fe, Ni, Cr and Mo in the solution, while the nickel implanted specimens yield significantly reduced concentrations. The greatest reduction of the ion concentrations in the solution is achieved with the implantation dose of 3×10^{17} ions cm^{-2}. In specific, Fe ions are reduced 9 times, Ni 38 times, Cr 37 times and Mo is even below the detectable level, compare to the bare SS316L. These data imply that good corrosion resistance is achieved by the nickel implantation, in good agreement with what the polarization curves (Fig. 5b) and the potentiostatic test results (Fig. 6) imply. The ICP results also confirm the same slight increase in the current density as we have already discussed for electrochemical results, for the specimens with implantation doses of 4×10^{17} or 5×10^{17} ions cm^{-2}. When the dose is increased to 5×10^{17} ions cm^{-2}, Fe, Ni, Cr and Mo ion concentrations are detected as 1.16, 0.14, 0.05 and 0.02 ppm, respectively, higher than those for the dose of 3×10^{17} ions cm^{-2}. The reason could be attributed to the increase of the flaws and defects created by over dose of ion implantation and the deteriorated surface integrity.

It is interesting to find that the ratio of the amount dissolved in the potentiostatic test to the concentration in the specimen for Ni is higher than that for Cr as measured from the XPS and ICP results, which imply that chromium oxide and hydroxide have lower corrosion rate compared with Ni and its oxide and hydroxide in the passive layer, as the oxide and hydroxide are the main species of the metallic elements. It is expected that Cr implantation on SS316L might improve the corrosion resistance to a higher extent.

3.4. Interfacial contact resistance

The interfacial contact resistance between the nickel implanted SS316L and the carbon paper was investigated as a function of compaction force (Fig. 7). ICR values for the bare 316L stainless steel and graphite were also measured for comparison. The typical compaction force in PEMFC is marked and the ICR value of all specimens is listed in Table 5 [3,8]. It can be seen from Fig. 7 that the ICR values decrease with increasing compaction force, as a result of the increasing contact points between the carbon paper and the stainless steel and the increasing actual conductive area [1]. The R_{base} follow the same trend, ranging from 12.2 mΩ at 30 N cm^2 to 1.4 mΩ at 360 N cm^{-2}. The ICR for the bare SS316L is higher than that for any nickel implanted SS316L over the whole range of applied compaction force. In particular, the ICR value for the bare SS316L is 312.8 mΩ cm^2 under the typical compaction force, and that for the Ni implanted with a dose of 1×10^{17} ions cm^{-2} is

Table 5
The ICR values for the bare and nickel implanted SS316L and graphite ($m\Omega\,cm^2$)

Bare SS316L	1×10^{17} Ni cm^{-2}	2×10^{17} Ni cm^{-2}	3×10^{17} Ni cm^{-2}	4×10^{17} Ni cm^{-2}	5×10^{17} Ni cm^{-2}	Graphite
312.8	36	119.5	131.8	155.3	263.3	5.4

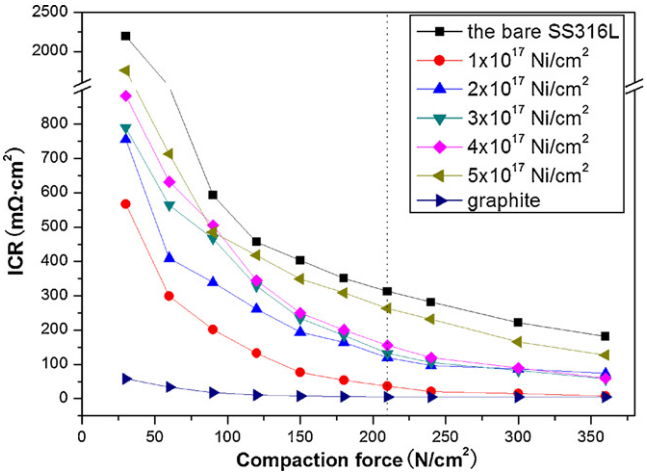

Fig. 7. Interfacial contact resistances between the bare and nickel implanted SS316L and the carbon paper at different compaction forces.

36 $m\Omega\,cm^2$, reduced by more than 8 times. The overall reduction in ICR by ion implantation is attributed to the change in the passive layer's thickness and the amounts of metallic species of Ni in this layer. The thickness is reduced from 50 to 18 nm and the metallic nickel is increased from 13 to 23%, compare with those of the bare specimen. The ICR for nickel implanted with a dose of 1×10^{17} ions cm^{-2} is the lowest and the ICR value increase with the dose of ion implantation in the applied pressure range. The variation of ICR with respect to the compaction forces is presumably related to the surface roughness that increases with increasing dose after the implantation, since the passive layer thickness remains the same and the amount of metallic Ni increases with increasing dose, which does not result in the increase of ICR. The actual ICR is influenced both by the contact area between the specimen and the carbon paper, and the local pressure on the contact spot that varies on a fluctuating surface, which is further influenced by the mechanical stiffness of the carbon paper. However, the detail of the mechanism has not been clarified, because an experimental quantification of these effects is difficult to carry out at the current stage.

4. Conclusions

The 316L stainless steel was nickel implanted for 1×10^{17}, 2×10^{17}, 3×10^{17}, 4×10^{17} and 5×10^{17} ions cm^{-2}, respectively. The potentiodynamic and potentiostatic test measured at 80 °C in 0.5 M H_2SO_4 with 2 ppm HF solution, and the ICP results, which are in agreement with each other, demonstrate that the corrosion resistance is improved by the formation of a Ni-rich surface layer with ion implantation. In particular, when nickel implanted with a dose of 3×10^{17} ions cm^{-2}, the corrosion potential (E_{corr}) moved to about −0.05 V versus SCE in the accelerate anode environment and the passivation current density reduced to 7 $\mu A\,cm^{-2}$, indicating that nickel implantation could greatly improve the corrosion resistance of SS316L in both anode and cathode environment. However, when the ion implantation was carried out for increased dose (for 4×10^{17} and 5×10^{17} ions cm^{-2}), the current density increased, indicating that the flaws and defects caused by the ion implantation deteriorated the Ni-rich layer's corrosion resistance. The nickel implantation could markedly decrease the interfacial contact resistance of SS316L due to the reduction in passive layer thickness.

Acknowledgement

The financial support provided by the National 863 Project of China under contract number 2006111A1222 and the National Science Foundation of China under contract number 50601018 is greatly appreciated.

References

[1] R.J. Tian, J.C. Sun, L. Wang, J. Power Sources 163 (2007) 719–724.
[2] T. Fukutsuka, et al., J. Power Sources 174 (2007) 199–205.
[3] K.M. Kim, K.Y. Kim, J. Power Sources 173 (2007) 917–924.
[4] R. Hornung, G. Kappelt, J. Power Sources 72 (1998) 20–21.
[5] J. Wind, R. Spah, W. Kaiser, G. Bohm, J. Power Sources 105 (2002) 256–260.
[6] J.S. Kim, W.H.A. Peleen, K. Hemmes, R.C. Makkus, Corros. Sci. 44 (2002) 635–655.
[7] H. Wang, J.A. Turner, J. Power Sources 128 (2004) 193–200.
[8] H. Wang, M.A. Sweikart, J.A. Turner, J. Power Sources 115 (2003) 243–257.
[9] I. Zafar, J. Guiheen, N. Dave, R. Timothy, World Patent WO00128019 (19 April 2001).
[10] T. Matsumoto, J. Niikura, H. Ohara, M. Uchida, H. Gyoten, K. Hatoh, E. Kanbara, K. Nishida, Y. Sugawara, European Patent EP 1094535 (25 April 2001).
[11] V.V. Nikam, R.G. Reddy, J. Power Sources 152 (2005) 146–155.
[12] V.V. Nikam, R.G. Reddy, Int. J. Hydrogen Energy 31 (2006) 1863–1873.
[13] S.-J. Lee, C.-H. Huang, J.-J. Lai, Yu-P. Chen, J. Power Sources 131 (2003) 243–257.
[14] Y. Wang, D.O. Northwood, J. Power Sources 165 (2007) 293–298.
[15] L. Ma, S. Warthesen, D.A. Shores, J. New Mater. Electrochem. Syst. 3 (2000) 221–228.
[16] M.P. Brady, K. Weisbrod, I. Paulauskas, R.A. Buchanan, K.L. More, H. Wang, M. Wilson, F. Garzon, L.R. Walker, Scripta Mater. 50 (2004) 1017–1022.
[17] J. Wind, R. Späh, W. Kaiser, G. Böhm, J. Power Sources 105 (2002) 256–260.
[18] V. Mehta, J.S. Cooper, J. Power Sources 114 (2003) 32–53.
[19] M. Xu, L. Li, Y. Liu, X. Cai, Q. Chen, P.K. Chu, Mater. Sci. Eng. A 425 (2006) 1–6.
[20] Y. Sugizaki, T. Yasunaga, H. Tomari, Surf. Coat. Technol. 83 (1996) 167–174.
[21] J.S. Kim, W.H.A. Peelen, K. Hemmes, R.C. Makkus, Corros. Sci. 44 (2002) 635–655.
[22] A.G. Duffy, L. Clapham, M.C. Ridgway, J.L. Whitton, Surf. Coat. Technol. 83 (1996) 189–193.
[23] H. Wang, G. Teeter, J.A. Turner, J. Electrochem. Soc. 152 (2005) B99.